


Effects of parietal suction and injection on the stability of the Blasius boundary-layer flow over a permeable, heated plate

Mushrifah Al-Malki ^{*}

*School of Mathematics and Actuarial Science, University of Leicester, Leicester LE1 7RH, UK
and Department of Mathematics and Statistics, Taif University, P. O. Box 888, Taif, Saudi Arabia*

Zahir Hussain [†] and Stephen Garrett [‡]

School of Engineering, University of Leicester, Leicester LE1 7RH, UK

Sophie Calabretto [§]

Department of Mathematics and Statistics, Macquarie University, Australia, NSW 2109



(Received 1 March 2021; accepted 12 October 2021; published 19 November 2021)

The main concern of this paper is to investigate the effects on the stability behavior of wall suction or injection for external boundary-layer flow over a heated, porous plate for a fluid with temperature-dependent viscosity. The wall suction or injection are applied to the flow by a simple modification for the no-penetration condition and the current boundary conditions on the flat plate. Liquid-type viscosities are found to entrain both the velocity and temperature profiles closer to the plate with increasing both temperature sensitivity and suction intensity, whereas gas-type viscosities are found to exhibit the reverse effect with increasing flow injection and decreasing temperature dependence. We present then the linear stability analysis and find that increasing both the temperature dependence (from gas- to liquid-type behavior) and suction intensity of the fluid leads to increasing critical Reynolds number to a point of maximum stability. We note also that increasing both the Prandtl number (Pr) and flow suction in the liquid-type behavior results in an increased critical Reynolds number. The magnitudes of the perturbation eigenfunctions are considered before utilising them to obtain solutions to an energy balance integral. We find that the eigenfunction profiles are imitative of the narrowing of their mean flow counterparts when increasing either the temperature dependence or the flow suction. Our results are then confirmed by the energy analysis, where we find a significant reduction in the energy produced by the disturbance with increasing suction intensity and ultimately leads to a more stable flow. Overall, there is a strong destabilizing effect with increasing injection and the temperature-dependent viscosity over a heated plate. In summary, the findings indicate that increasing the wall suction and temperature dependence results in significantly more stable flows. It is worth noting that application and extension of this study are considered in the context of chemical vapor deposition reactors.

DOI: [10.1103/PhysRevFluids.6.113902](https://doi.org/10.1103/PhysRevFluids.6.113902)

*masam2@leicester.ac.uk

†zahir.hussain@leicester.ac.uk

‡stephen.garrett@leicester.ac.uk

§sophie.calabretto@mq.edu.au

I. INTRODUCTION

The laminar transition of external flow to turbulence with parietal suction or injection is a widely important phenomenon in many physical flows, such as engineering processes and industrial systems. Some of the important applications for injection are gas turbines and turbojets. The effect of injection on flow stability has been studied by Thierry and Grégoire [1]. Meanwhile, boundary-layer separation is controlled by suction in aerodynamic applications for instance in laminar flow control of internal and external flows.

There are a number of studies which are concerned on these occurrences spanning recent decades, which have looked at the boundary-layer disturbances via external agents, for example free-stream fluctuations and whether these turbulent-transition effects become unstable and lead to the laminar flow breakdown [2]. There is no doubt that this interest is due to the significant problems in fluid flow mechanics wherein most technological applications, skin-friction drag has become a greater issue in the transition to turbulence, and the delay of transition is of particular interest. Therefore the stabilization of laminar flows have been investigated extensively, interesting examples include roughness levels, suction, mean flow distortion and wave cancellation by superposition [3–5], as intelligent strategies to delay the laminar-turbulent transition process of flow.

Recent studies have focused exclusively on examining the effects of suction or blowing on the turbulent boundary layer flows [6–9]. Park and Choi [10] numerically investigated the effects of uniform suction or blowing on a turbulent boundary layer flow which has a spanwise slot. This study showed that the skin friction and turbulence intensities above the slot and also downstream of the slot change significantly using small-magnitude uniform suction or injection. The authors noted that recovering from both cases of suction or injection occurs rapidly, while recovering from other turbulence intensities and shear stress requires a longer distance downstream.

Examining the effect of injection velocity using three values of the injection intensity as direct numerical simulations on the characteristics of the boundary-layer turbulence has been conducted by Kim *et al.* [11]. Pantokratoras [12] investigated the problem of laminar-free convection over a vertical isothermal plate in the temperature range between 20 °C and 0 °C with uniform blowing or suction in water taking into consideration the temperature dependence of viscosity and density. This work indicated that the variation of such parameters with temperature has a strong impact on the results of the numerical solution of the boundary-layer equations. Bansal [13] has investigated thermal boundary layers and the velocities over a porous flat plate with variable suction, or injection velocity, and also considered constant wall temperature, without restricting the scope of the Prandtl number. The author pointed out that this research has limiting cases of zero and asymptotic suction for velocity and thermal boundary layers. Mohamed Ali [14] presented the similarity solutions for laminar boundary-layer equations on a stretching surface with suction or injection. The results of this examination show that the suction of the boundary-layer acts to delay the back flow over the stretching surface, while injection intensity leads to increasing the strength of the reverse flow. Hossaina *et al.* [15] considered the boundary layer flow of the unsteady laminar combining free and enforced convective in viscous incompressible fluid with suction and injection about a vertical porous plate. The authors showed that a small amount of suction or blowing plays a great role in the velocity of flow and temperature distributions. Abu Bakara *et al.* [16] studied numerically the influence of suction on the steady boundary-layer flow over a stretching or shrinking cylinder. Meanwhile, Laouar and Mezaache [17] have studied the effects of parietal suction and blowing with viscosity on the hydrodynamic and thermal behavior of external flow. They demonstrated that the momentum and heat transfer can be significantly affected by wall conditions. The function of the imposed stream condition for laminar flow produces the flow similarity for both cases of suction and injection. Contrary to that, turbulent flow parameters are a strongly dissimilar. Shojaefard *et al.* [18] presented a numerical study concerning flow control by suction and injection for the aerodynamic characteristics of a specific airfoil. Their conclusions reveal that the suction slots near the trailing edge can greatly increase the lift coefficient, while the injection decreases the skin friction. Laouar *et al.* [19] focused on the temporal linear stability characteristics of laminar forced-convection

external flows along a horizontal permeable flat plate. The findings of this study illustrate that increasing the intensity of suction or decreasing the intensity of blowing raises the critical Reynolds number.

The Blasius boundary layer has been considered a staple of fluid mechanics since the early 20th century [20]. The first studies of the effects of small disturbances on the laminar flow over a flat plate were by Tollmien [21] and Schlichting [22], where they considered the amplification of linear, wavelike disturbances as the key mechanism for unstable flows. The ability to identify a critical Reynolds number, which is the specific point of the beginning of transition from the laminar to turbulent regime, was a particularly useful result from this work. The existence of Tollmien-Schlichting (T-S) waves were demonstrated by Schubauer [23], who observed the waves for the first time during experiments in a heavily damped wind tunnel.

The work presented will analyze the effects of wall suction and injection to chemical vapor deposition (CVD): a microfabrication process where a gas mixture is pumped into a reactor and flows over a heated reactant porous surface to chemically deposit a thin film of material. For promoting regular and cohesive film growth, laminar flow must be maintained in a CVD reactor, where the deposition process could be disrupted by turbulent or unstable flows [24,25].

It is possible that the sharp temperature gradients in a CVD reactor produce variations in all physical properties of the fluid as presented in Refs. [26,27], and therefore there is a need for a temperature-dependent viscosity model. Miller *et al.* [28] represents the first step to analyzing the larger stability of flows in CVD reactors on a smooth surface of flat plate. Our paper will expand Miller *et al.* [28] to include wall suction and injection that have been shown in Laouar *et al.* [19], which are applied to analyze the effects of parietal suction and injection on the stability of flows in a CVD reactor.

This study is organized as follows: Section I is a brief introduction to the smooth flat plate with temperature-dependent viscosities of boundary-layer flows. In Sec. II, the governing steady mean flow equations of the heated plate problem are formulated with the effects of the wall suction or injection further analyzed and discussed. In Secs. III and IV, the linear stability properties of the resulting steady flows are investigated wherein the neutral curves, critical Reynolds numbers, growth rates, and amplitude ratios for different intensities of the suction or injection are presented. In Sec. V, an analysis of the energy balance within the boundary-layer flow is analyzed for extracting possible underlying physical mechanisms behind the impacts of wall suction or injection on the flow stability. Finally, in Sec. VI, the summary and conclusions are drawn.

A. The physical model

A schematic diagram of the physical model taken into account is shown in Fig. 1. It consists of a permeable, heated wall in direct contact with laminar and turbulent external flow. Wall heating, flow suction, and injection induce momentum and heat transfer. The physical model is two dimensional. The coordinate system Oxy is located on the flat plate and defined thus: Ox axis is in the flow direction and Oy axis is normal to the plate and directed toward the flow.

II. MEAN FLOW OF A HEATED PLATE WITH WALL SUCTION AND INJECTION

A. Formulation

We consider a steady, incompressible, Newtonian fluid flowing with velocity $\mathbf{U}^* = (U^*, V^*)$ over a semi-infinite flat, porous plate, where U^* and V^* are the velocities in the streamwise and plate-normal directions x^* and y^* , respectively. Here T^* is the temperature of the fluid, and the plate heated to a fixed temperature T_w^* . Note that the dimensional quantities here are denoted by asterisk superscripts.

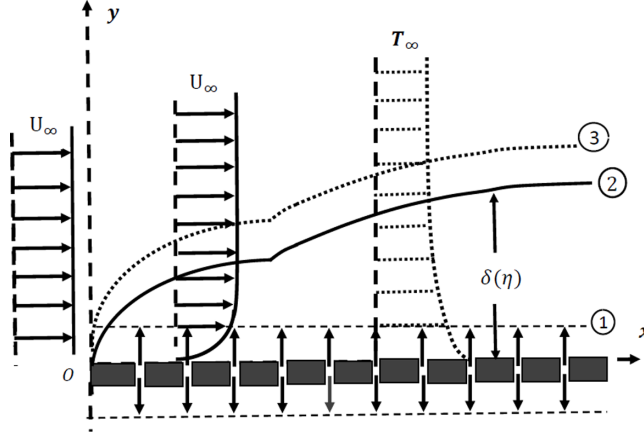


FIG. 1. Schematic diagram of the physical model. Wall suction (\downarrow) or injection (\uparrow). Adapted from Laouar and Mezaache [17], (1) wall with suction or injection, (2) dynamic laminar/turbulent boundary layer, and (3) thermal boundary layer

The system is governed by the following mass, momentum, and heat continuity equations:

$$\nabla^* \cdot \mathbf{U}^* = 0, \quad (1)$$

$$\left(\frac{\partial}{\partial t^*} + \mathbf{U}^* \cdot \nabla^* \right) \mathbf{U}^* = -\frac{1}{\rho^*} \nabla^* p^* + \frac{1}{\rho^*} \nabla^* \cdot \boldsymbol{\tau}^*, \quad (2)$$

$$\rho^* C_p^* \left(\frac{\partial}{\partial t^*} + \mathbf{U}^* \cdot \nabla^* \right) T^* = k^* \nabla^{*2} T^*, \quad (3)$$

where ρ^* is the fluid density, t^* is the time, p^* is the pressure, C_p^* is the specific heat capacity of the fluid, and k^* is the heat diffusion constant. The viscous stress tensor is given by $\boldsymbol{\tau}^* = \mu^* \dot{\boldsymbol{\gamma}}^*$, where $\dot{\boldsymbol{\gamma}}^* = \nabla^* \mathbf{U}^* + (\nabla^* \mathbf{U}^*)^T$ is the rate-of-strain tensor. Equation (3) is coupled to (1) and (2) via the temperature dependence of the fluid viscosity,

$$\mu^* = \mu_{\infty}^* [1 + \varepsilon^* (T^* - T_{\infty}^*)]^{-1},$$

where μ_{∞}^* and T_{∞}^* represent the free-stream viscosity and temperature, respectively. The sensitivity of viscosity to changes in temperature is represented by the characteristic constant of fluid ε^* . As will be considered for a heated plate, i.e., $T_w^* > T_{\infty}^*$, the case of $\varepsilon^* < 0$ represents the viscothermal behavior of a gas, while the case $\varepsilon^* > 0$ represents that of a liquid. Setting $\varepsilon^* = 0$ indicates a constant viscosity and uncouples (3) from (1) and (2).

The nondimensional variables scales of the system are introduced as follows:

$$\begin{aligned} \mathbf{U}^* &= U_{\infty}^* (U, V), & (x^*, y^*) &= L^* (x, y), & t^* &= (L^*/U_{\infty}^*) t, \\ p^* &= \rho^* U_{\infty}^{*2} p, & T^* - T_{\infty}^* &= T (T_w^* - T_{\infty}^*), & \varepsilon^* &= \varepsilon / (T_w^* - T_{\infty}^*). \end{aligned}$$

Here U_{∞}^* is the free stream velocity, L^* is the length scale, δ is the scaling constant of the boundary layer, and ε is the nondimensional temperature dependence parameter. From the

equations (1)–(3), the nondimensional system of equations becomes then

$$\frac{\partial U}{\partial x} + \frac{\partial V}{\partial y} = 0, \quad (4)$$

$$\left(\frac{\partial}{\partial t} + U \frac{\partial}{\partial x} + V \frac{\partial}{\partial y} \right) U = -\frac{\partial p}{\partial x} + \frac{1}{\text{Re}} \left[\mu \nabla^2 U + \frac{\partial \mu}{\partial y} \left(\frac{\partial U}{\partial y} + \frac{\partial V}{\partial x} \right) + 2 \frac{\partial \mu}{\partial x} \frac{\partial U}{\partial x} \right], \quad (5)$$

$$\left(\frac{\partial}{\partial t} + U \frac{\partial}{\partial x} + V \frac{\partial}{\partial y} \right) V = -\frac{\partial p}{\partial y} + \frac{1}{\text{Re}} \left[\mu \nabla^2 V + \frac{\partial \mu}{\partial x} \left(\frac{\partial U}{\partial y} + \frac{\partial V}{\partial x} \right) + 2 \frac{\partial \mu}{\partial y} \frac{\partial V}{\partial y} \right], \quad (6)$$

$$\left(\frac{\partial}{\partial t} + U \frac{\partial}{\partial x} + V \frac{\partial}{\partial y} \right) T = \frac{1}{\text{RePr}} \nabla^2 T, \quad (7)$$

where $\mu = (1 + \varepsilon T)^{-1}$, $\text{Re} = U_\infty^* L^* \rho^* / \mu_\infty^*$ is the Reynolds number, and $\text{Pr} = C_p^* \mu_\infty^* / k^*$ is the Prandtl number. In this work, we set $\text{Pr} = 0.72$, which is consistent for a range of gases, including air. The effect of varying the Prandtl number is also considered for a liquid-type viscosity.

We consider the physical model shown above in Sec. I. The boundary conditions are then defined as

$$y = 0, \quad U = 0 \quad \text{and} \quad T = 1, \quad \text{as} \quad y \rightarrow \infty, \quad U \rightarrow 1 \quad \text{and} \quad T \rightarrow 0.$$

We have a small parameter which is $\delta = O(\text{Re}^{-1/2})$, at the boundary-layer region close to the surface of the plate. We define also the boundary-layer coordinate: $\eta = y/\sqrt{x}$, hence the following similar variables are formulated

$$U = f'(\eta), \quad V = [\eta f'(\eta) - f(\eta)]/2\sqrt{x}, \quad T = \Theta(\eta), \quad (8)$$

where the primes indicate differentiation with respect to η .

We substitute Eq. (8) into the system (4)–(7), we then obtain the mean-flow equations as follows:

$$(\bar{\mu} f'')' + \frac{1}{2} f f'' = 0, \quad (9)$$

$$\Theta'' + \frac{1}{2} \text{Pr} f \Theta' = 0, \quad (10)$$

where $\bar{\mu} = (1 + \varepsilon \Theta)^{-1}$. Equations (9) and (10) are a boundary-value problem which is solved using numerical methods subject to the modified wall boundary conditions which are expressed as

$$f(0) = f_w, \quad f'(0) = 0, \quad \Theta(0) = 1, \quad (11)$$

$$f'(\eta \rightarrow \infty) = 1, \quad \Theta(\eta \rightarrow \infty) \rightarrow 0. \quad (12)$$

Here primes denote differentiation with respect to η , the wall stream function $f_w > 0$ represents wall suction, and $f_w < 0$ indicates injection. These boundary conditions change to the boundary conditions for a smooth, impermeable plate. The solutions converge at $\eta = 20$ to a tolerance of 10^{-8} ; we consider this numerical representation of free-stream conditions as $\eta \rightarrow \infty$. Note that η is the similarity coordinate and $f(\eta)$ the nondimensional stream function.

The effect of ε on the boundary layer thickness δ^* is noted by measuring the Blasius constant δ , given as follows:

$$\delta = \int_0^\infty (1 - U) d\eta = \delta^* \sqrt{\frac{\rho^* U_\infty^*}{\mu_\infty^* x^*}}. \quad (13)$$

B. Results of temperature-dependent viscosity with wall suction and injection

From Eq. (11), we note that imposing outward parietal velocity acts to produce flow suction, represented by positive values of stream function. Figure 2 shows the viscosity profiles of $\bar{\mu}(\eta)$ with

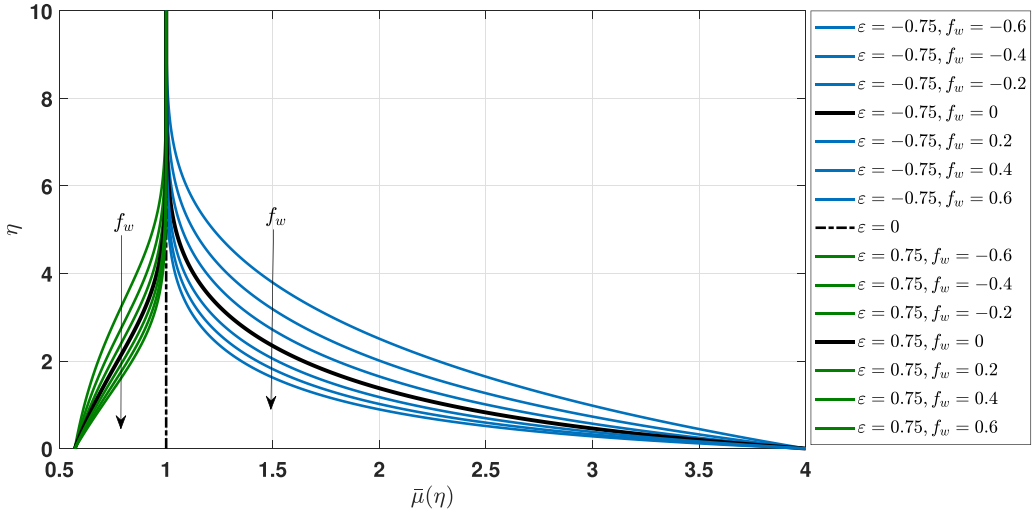


FIG. 2. Mean flow profiles, viscosity profiles $\bar{\mu}(\eta)$, in the cases of various suction and injection, and a range of temperature dependencies.

various intensities of the flow suction over a heated plate. Figure 2 presents viscosity profiles for a range of flow suction $f_w > 0$ and temperature dependencies. The boundary layers of the viscosity profiles narrow strongly with increasing the suction intensity and are closer to the surface plate. Figures 3 and 4 present viscosity profiles for a range of temperature dependencies and at fixed suction and injection intensities, respectively. For Fig. 3, the viscosity profiles move in a gradual reduction of $\bar{\mu}(\eta)$ as $f_w > 0$ and $\varepsilon > 0$, including a greater narrowing to both sides of the viscosity $\mu(\eta \rightarrow \infty) = 1$, which is due to the uniform temperature in the free stream. In all three cases of flow suction, we see that $\bar{\mu}(\eta)$ is equal to the value one for the temperature independent case $\varepsilon = 0$. This means that the fluid viscosity is in the free stream, and hence it is not affected by wall suction when $\varepsilon = 0$.

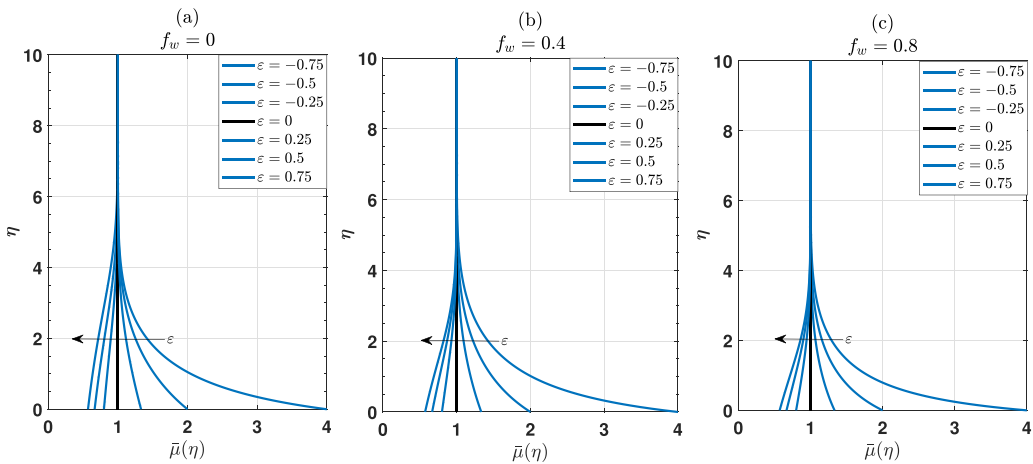


FIG. 3. Mean flow profiles, viscosity profiles $\bar{\mu}(\eta)$. (a) $f_w = 0$ and a range of ε , (b) $f_w = 0.4$ and a range of ε , and (c) $f_w = 0.8$ and a range of ε .

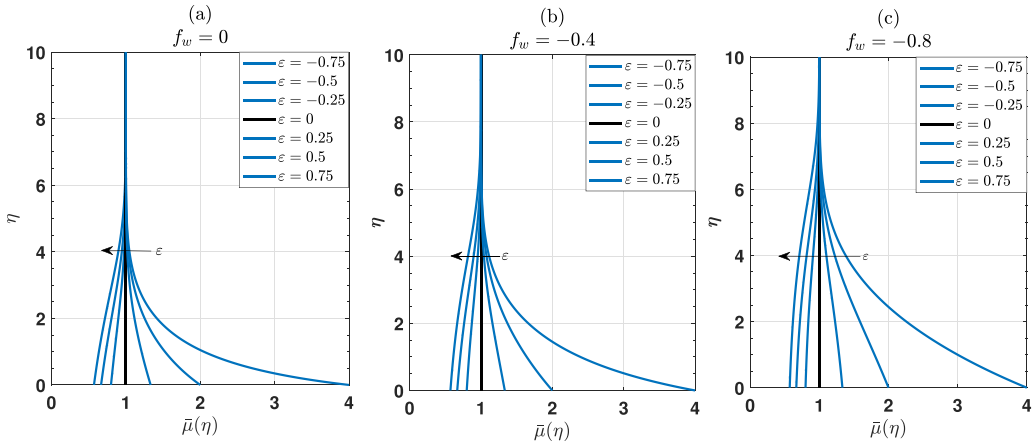


FIG. 4. Mean flow profiles, viscosity profiles $\bar{\mu}(\eta)$. (a) $f_w = 0$, and a range of ϵ . (b) $f_w = -0.4$, and a range of ϵ . (c) $f_w = -0.8$, and a range of ϵ .

The plots in Figs. 5–7 present the mean flow solutions of the velocity and temperature profiles for a range of the suction values with three constant values of $\epsilon = -0.75, 0, 0.75$, respectively. Figures 5(a), 6(a), and 7(a) show the velocity profiles of $U(\eta)$ for the case of different suction intensities at a fixed temperature dependence $\epsilon = -0.75, 0, 0.75$. Increasing both f_w and ϵ results in a greater thinning of the boundary layer and the velocity profiles are shifted toward the plate surface and the boundary-layer edge. In Figs. 5(b), 6(b), and 7(b), the velocity gradient takes a maximum value at the plate surface and a higher narrowing in the boundary layer is observed as a result of increasing the suction intensity and ϵ . In contrast, decreasing ϵ slightly broadens the boundary layers of the mean velocity profiles of $U(\eta)$ and $U'(\eta)$ as observed in Figs. 5(a) and 5(b). Therefore, lower values of $U'(\eta)$ profiles are noted.

Regarding Figs. 5(c), 6(c), and 7(c), show a gradual reduction in the temperature profiles toward the plate surface as f_w and ϵ are increased. However, this reduction decreases significantly when decreasing ϵ as seen in Fig. 5(c).

From Table I, we note that increasing the suction f_w and ϵ also decreases δ . Due to the dependence of the boundary layer (δ) on U , it can be inferred that the narrowing of the boundary layer results in the narrowing of the mean velocity profile.

The velocity profiles obtained for $\epsilon = 0$ in this study are compared with a surprisingly simple solution reported in Ref. [29], which is obtained in the case of a flat plate at zero incidence with uniform suction, and we note that our results have a good agreement with the result observed by Schlichting [29].

In contrast, we find also that flow injection is produced by imposing an inward parietal velocity represented by negative values of the wall stream function. Figure 2 shows the viscosity profiles of $\bar{\mu}(\eta)$ with various intensities of injection over a heated, permeable plate. Figure 2 presents viscosity profiles for a range of injection intensities $f_w < 0$ and ϵ . Increasing the intensity of injection makes the boundary layers of the viscosity profiles thicker and more distant from the surface plate, especially with increasing viscosity ($\epsilon < 0$). Figure 4 presents the viscosity profiles for a range of temperature dependencies and a fixed injection intensity of $f_w = 0, f_w = -0.4$, and $f_w = -0.8$, respectively. These cases display a gradual reduction in height of $\bar{\mu}(\eta)$ profiles away from the surface for $f_w < 0$, as the temperature-dependent viscosity is increased from negative.

We find that the dimensionless velocity increases with increased injection, which is evident from the plots in Figs. 5(a), 6(a), and 7(a) of the velocity profile, $U(\eta)$ for a range of the injection values with three constant values of $\epsilon = -0.75, 0, 0.75$, respectively. We found that increasing the injection strength results in a significant thickening of the boundary layer and causes the velocity

TABLE I. Computed mean flow data for a range of temperature dependencies for flow suction and injection at fixed ε values.

f_w	$U'(0)$	$\Theta'(0)$	δ
$\varepsilon = -0.75$			
-0.6	0.0547	-0.10196	3.9656
-0.4	0.0692	-0.14470	3.4302
-0.2	0.0848	-0.19207	3.0083
0	0.1016	-0.24306	2.6688
0.2	0.1192	-0.29691	2.3909
0.4	0.1376	-0.35306	2.1599
0.6	0.1568	-0.41109	1.9653
$\varepsilon = 0$			
-0.6	0.1349	-0.14182	2.6882
-0.4	0.1956	-0.19112	2.2674
-0.2	0.2616	-0.24247	1.9587
0	0.3321	-0.29564	1.7208
0.2	0.4061	-0.35042	1.5313
0.4	0.4833	-0.40665	1.3767
0.6	0.5630	-0.46419	1.2481
$\varepsilon = 0.75$			
-0.6	0.1475	-0.15369	2.3378
-0.4	0.2487	-0.20921	1.8759
-0.2	0.3622	-0.26452	1.5670
0	0.4853	-0.32023	1.3429
0.2	0.6160	-0.37660	1.1719
0.4	0.7529	-0.43377	1.0370
0.6	0.8949	-0.49177	0.9278

profile to move far away from the plate surface. In Figs. 5(b), 6(b), and 7(b), the inflectional nature of $U'(\eta)$ increases to a maximum at some distance away from the plate surface and a higher thickness in the boundary layer as a result of increasing injection intensity and decreasing ε , as seen in Fig. 5.

Figures 5(c), 6(c), and 7(c) show an increase in the temperature profile gradients far away from the plate surface with $f_w < 0$. This increase is greater with decreasing ε as seen in Fig. 5(c).

From Table I, we can see that increasing the injection strength f_w and decreasing or increasing ε also increases the thickness of the boundary layer. This is due to the dependence of the boundary layer (δ) on U . It can be inferred that the thickness of the boundary layer also causes the thickness of the mean velocity profile. Our results are in agreement with Laouar *et al.* [19] and Miller *et al.* [28].

We now consider the Prandtl number, a dimensionless quantity approximating the ratio of momentum diffusivity to thermal diffusivity. Note that the temperature-dependent viscosity of the fluid is increased with increasing temperature dependence ($\varepsilon < 0$) for air and gasses, and therefore the momentum diffusivity rate will be decreased. This means that the thermal diffusivity is dominant, and hence $Pr \ll 1$. Meanwhile, the viscosity decreases with increasing temperature dependence ($\varepsilon > 0$) for liquids, this could make the viscous diffusion rate dominant, so $Pr \gg 1$. This leads us to examine the effect of increasing Pr and wall suction intensity in a liquid-type viscosity, $\varepsilon > 0$, where we find that there is an extremely slight change in the velocity profile as it is evident in Figs. 8(a) and 8(c). However, the temperature profile shows a greater reduction toward the plate when increasing both Pr and wall suction intensity as seen in Figs. 8(b) and 8(d).

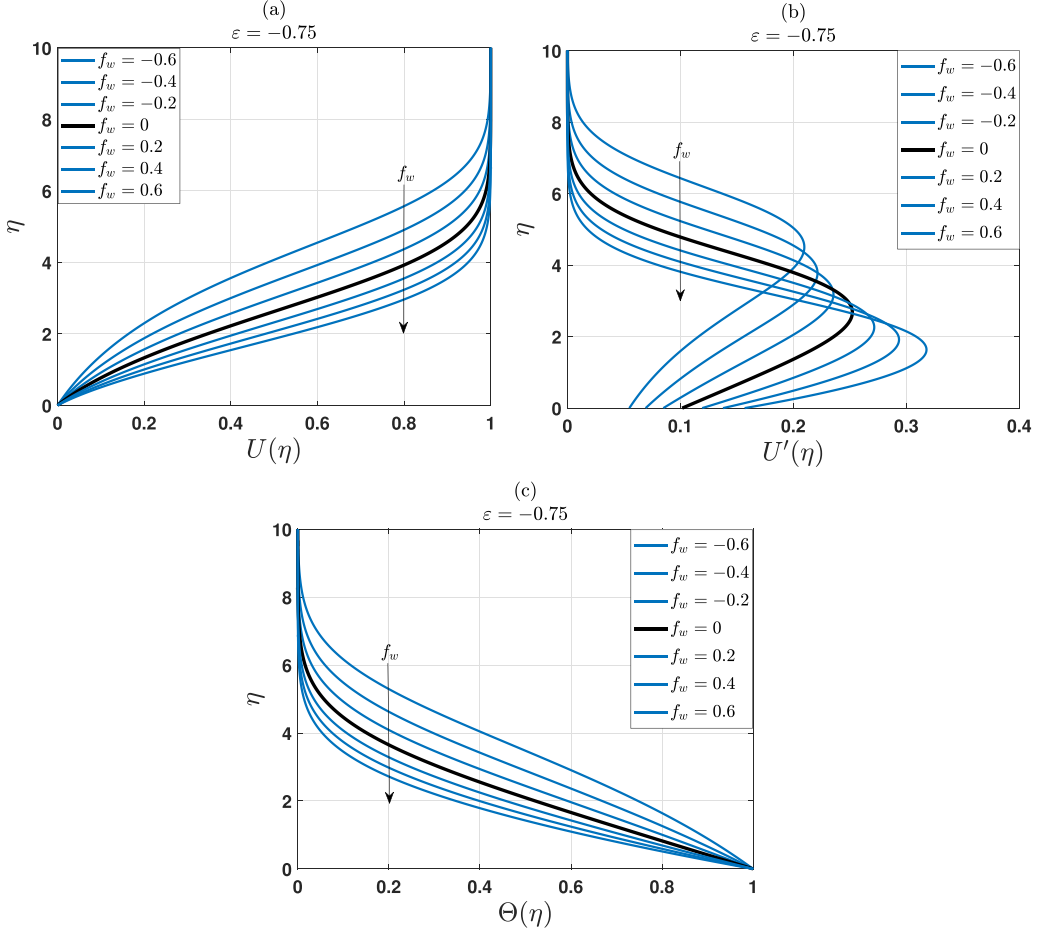


FIG. 5. Mean flow profiles, in cases of various suction and injection, and fixed $\varepsilon = -0.75$. (a) streamwise velocity, (b) velocity gradient, and (c) temperature.

III. LINEAR STABILITY EQUATIONS

A. Formulation

A small perturbation quantity is added to each of the mean flow variables

$$u(x, y, t) = U(x, y) + \hat{u}(x, y, t), \quad (14)$$

$$v(x, y, t) = \text{Re}^{-1/2}V(x, y) + \hat{v}(x, y, t), \quad (15)$$

$$p(x, y, t) = p(x) + \hat{p}(x, y, t), \quad (16)$$

$$T(x, y, t) = \Theta(x, y) + \hat{\Theta}(x, y, t). \quad (17)$$

In order to derive the governing set of disturbance equations used in the forthcoming numerical analysis, the quantities in Eqs. (1)–(3) are nondimensionalized with the same velocity, length, time, pressure, and temperature scales shown in Sec. II B, where L^* is taken to be δ^* , then we have

$$(x^*, y^*) = \delta^*(x, y), \quad t^* = (\delta^*/U_\infty^*)t.$$

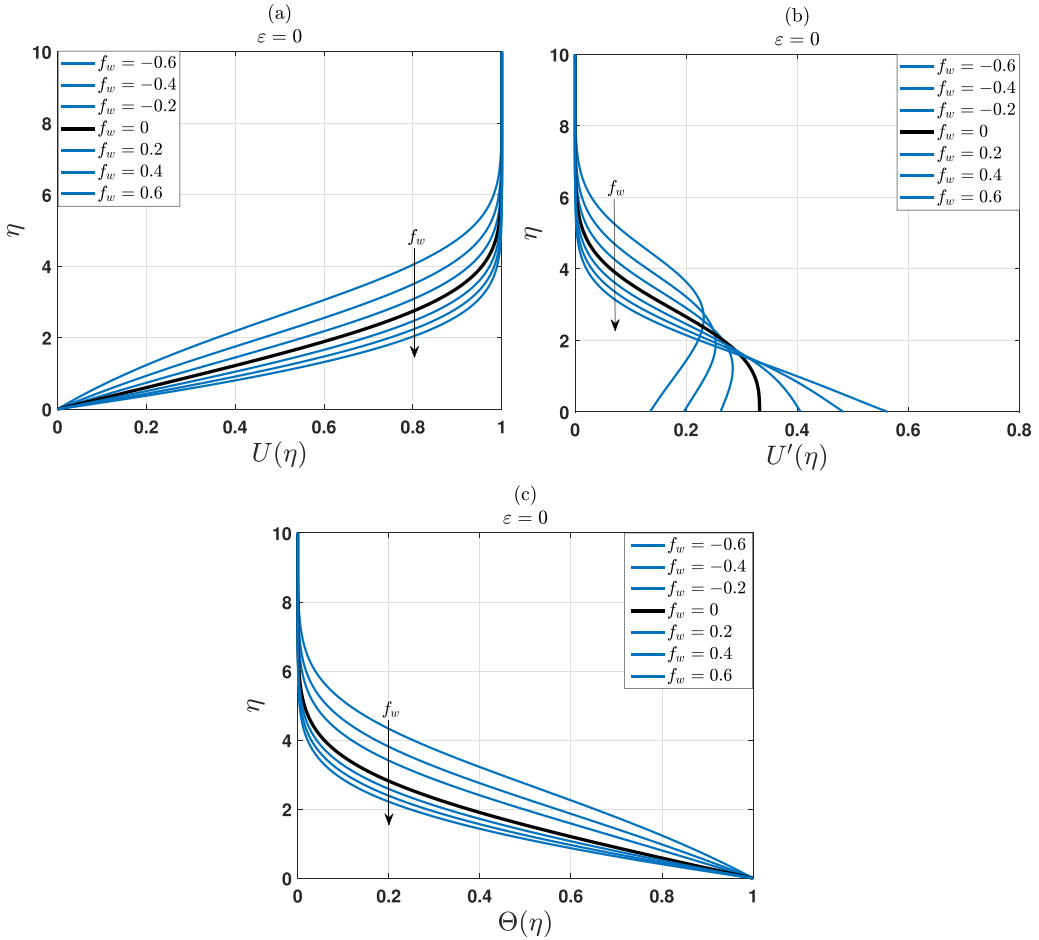


FIG. 6. Mean flow profiles, in cases of various suction and injection, and fixed $\varepsilon = 0$. (a) Streamwise velocity, (b) velocity gradient, and (c) temperature.

Note here that the choice of scaling is identical with the exception of the length and time scales, which are now scaled in relation to the boundary-layer thickness δ^* . At this point the newly scaled Reynolds number is defined as

$$R = \delta \sqrt{x \text{Re}}.$$

The perturbed base flow (14)–(17) is then substituted into the resulting system of equations. A “parallel-flow approximation” is imposed by the disturbances considered to occur sufficiently downstream ($x \gg 1$) such that we ignore streamwise boundary-layer growth. Recalling that $V(x, y) \propto x^{-1/2}$ acts to assume that $V \ll 1$. Therefore, the mean flow variables $U(y)$ and $\Theta(y)$ are now functions of y alone. The viscosity μ has undergone a Taylor expansion to first order to retain the mean flow form

$$\mu \approx \frac{1}{1 + \varepsilon \Theta} - \frac{\varepsilon \hat{\Theta}}{(1 + \varepsilon \Theta)^2} = \bar{\mu} + \hat{\mu},$$

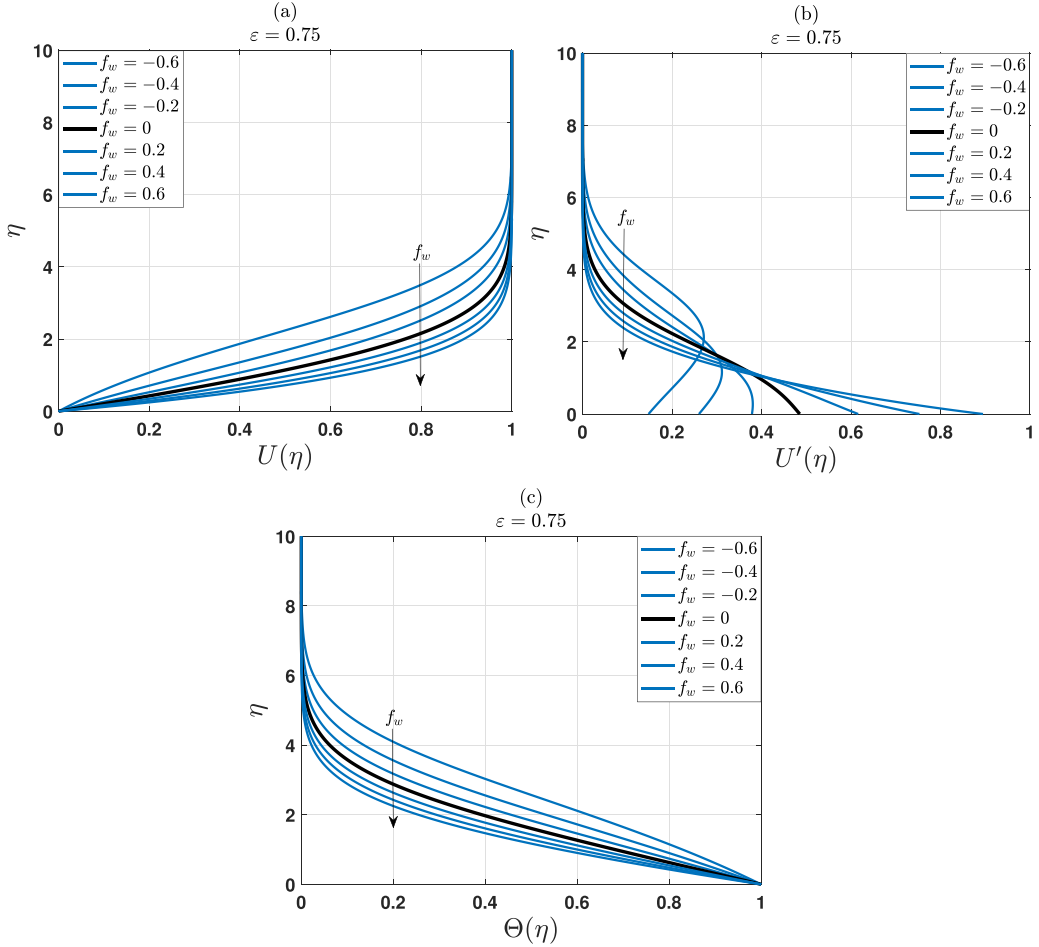


FIG. 7. Mean flow profiles, in cases of various suction and injection, and fixed $\varepsilon = 0.75$. (a) Streamwise velocity, (b) velocity gradient, and (c) temperature.

where $\hat{\mu} = -\varepsilon\bar{\mu}^2\hat{\Theta}$. We now obtain the following system of PDEs that are separable in x and t :

$$\frac{\partial \hat{u}}{\partial x} + \frac{\partial \hat{v}}{\partial y} = 0, \quad (18)$$

$$\frac{\partial \hat{u}}{\partial t} + U \frac{\partial \hat{u}}{\partial x} + U' \hat{v} = -\frac{\partial \hat{p}}{\partial x} + \frac{\bar{\mu}}{R} \left(\frac{\partial^2 \hat{u}}{\partial x^2} + \frac{\partial^2 \hat{u}}{\partial y^2} \right) + \frac{\bar{\mu}}{R} \left(\frac{\partial \hat{v}}{\partial x} + \frac{\partial \hat{u}}{\partial y} \right) + \frac{U'' \hat{\mu}}{R} + \frac{U' \partial \hat{\mu}}{R \partial y}, \quad (19)$$

$$\frac{\partial \hat{v}}{\partial t} + U \frac{\partial \hat{v}}{\partial x} = -\frac{\partial \hat{p}}{\partial y} + \frac{\bar{\mu}}{R} \left(\frac{\partial^2 \hat{v}}{\partial x^2} + \frac{\partial^2 \hat{v}}{\partial y^2} \right) + \frac{2\bar{\mu}' \partial \hat{v}}{R \partial y} + \frac{U' \partial \hat{\mu}}{R \partial x}, \quad (20)$$

$$\frac{\partial \hat{\Theta}}{\partial t} + U \frac{\partial \hat{\Theta}}{\partial x} + \Theta' \hat{v} = \frac{1}{RPr} \left(\frac{\partial^2 \hat{\Theta}}{\partial x^2} + \frac{\partial^2 \hat{\Theta}}{\partial y^2} \right). \quad (21)$$

The perturbation quantities are then expressed in terms of normal modes

$$(\hat{u}, \hat{v}, \hat{p}, \hat{\Theta}) = (\tilde{u}, \tilde{v}, \tilde{p}, \tilde{\Theta}) e^{i(\alpha x - \omega t)}.$$

Here $\alpha = \alpha_r + i\alpha_i$ is the complex streamwise wave number and ω is the real disturbance frequency. In the case that $\alpha_i < 0$, the disturbance is convectively unstable and grows downstream. The

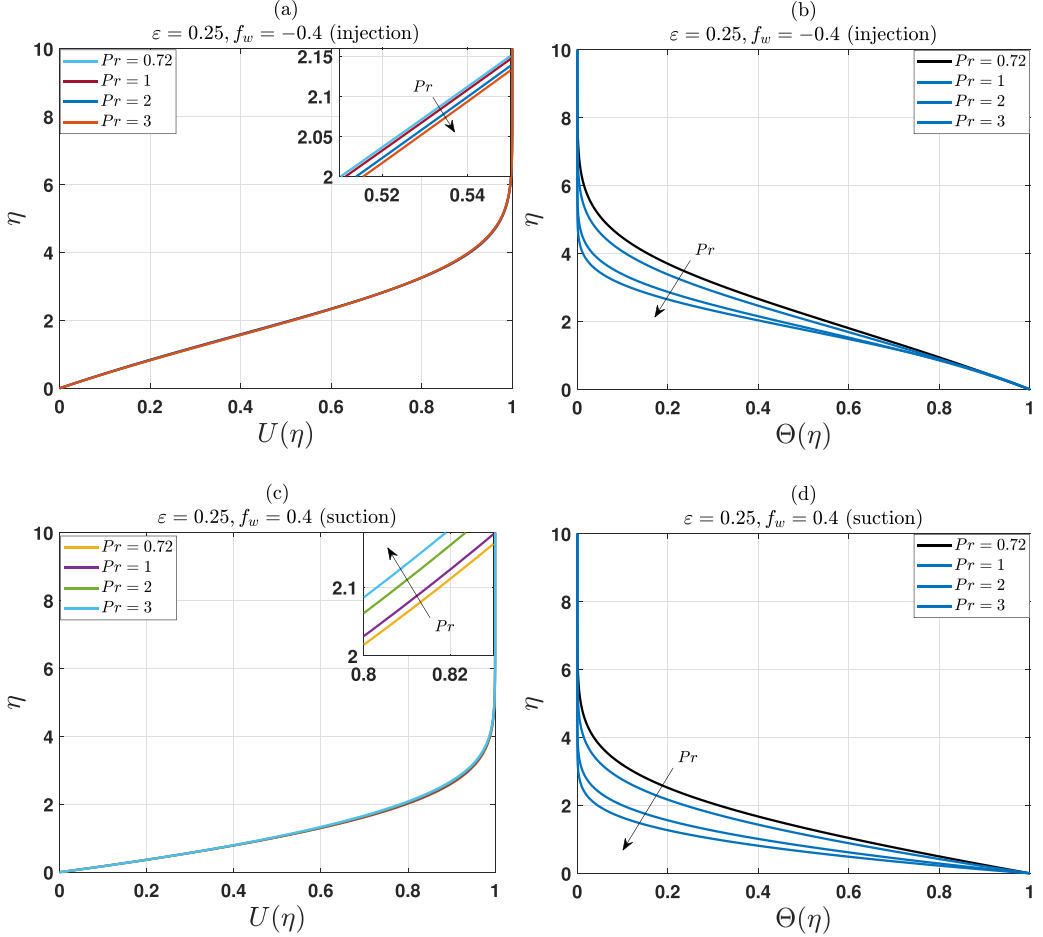


FIG. 8. Mean flow profiles of a range of Prandtl number values, and at a fixed value of $\varepsilon = 0.25$, and fixed values of $f_w = -0.4, 0.4$. (a) Streamwise velocity for injection, (b) temperature profile for injection, (c) axial velocity for suction, and (d) temperature for suction.

perturbation quantities in Eqs. (18)–(21) are now expressed in their normal mode form, producing the resulting system of stability equations

$$i\alpha\tilde{u} + \tilde{v}' = 0, \quad (22)$$

$$R[i(\alpha U - \omega)\tilde{u} + U'\tilde{v} + i\alpha\tilde{p}] = \bar{\mu}(\tilde{u}'' - \alpha^2\tilde{u}) - \varepsilon\bar{\mu}^2[\Theta'(\tilde{u}' + i\alpha\tilde{v}) + (U'\tilde{\Theta})'] + 2\varepsilon^2\bar{\mu}^3U'\Theta'\tilde{\Theta}, \quad (23)$$

$$R[i(\alpha U - \omega)\tilde{v} + \tilde{p}'] = \bar{\mu}(\tilde{v}'' - \alpha^2\tilde{v}) - \varepsilon\bar{\mu}^2[2\Theta'\tilde{v}' + i\alpha U'\tilde{\Theta}], \quad (24)$$

$$\text{Pr}R[i(\alpha U - \omega)\tilde{\Theta} + \Theta'\tilde{v}] = \tilde{\Theta}'' - \alpha^2\tilde{\Theta}. \quad (25)$$

Note that in the limit as $\varepsilon \rightarrow 0$ this system can be reduced to the classical fourth-order Orr-Sommerfeld equation. The system (22)–(25) is solved as a quadratic eigenvalue problem of the form $A_2\alpha^2 + A_1\alpha + A_0 = \tilde{Q}$, where $\tilde{Q} = (\tilde{u}, \tilde{v}, \tilde{p}, \tilde{\Theta})^T$ is the vector of eigenfunctions, and the

quantities A_j are matrices containing the coefficients of the $O(\alpha^j)$ terms. The eigenfunctions are then computed according to the boundary conditions

$$\tilde{u}(y=0) = \tilde{v}(y=0) = \tilde{v}'(y=0) = \tilde{p}(y=0) = \tilde{\Theta}(y=0) = 0, \quad (26)$$

$$\tilde{u}(y \rightarrow \infty) = \tilde{v}(y \rightarrow \infty) = \tilde{p}(y \rightarrow \infty) = \tilde{\Theta}(y \rightarrow \infty) \rightarrow 0. \quad (27)$$

We obtain the neutral temporal and spatial stability solutions via a Chebyshev polynomial discretization method. An exponential map is used to transform the Gauss-Lobatto collocation points into the physical domain. We solve then the stability equations as primitive variables over 100 the collocation points distributed between the upper and lower boundaries, with the exception of the boundary conditions in Eqs. (26) and (27), which are imposed at $y = 0$ and $y = y_{\max}$, where suitable mean-flow convergence is again found at $y_{\max} = 20$.

B. Neutral stability curves results for flow suction or injection

The solutions of the system (22)–(25) are the points on the neutral curves, when $\alpha_i = 0$. The region enclosed by the neutral curve identifies unstable points of the flow for which a disturbance exponentially grows as $\alpha_i < 0$, while the region which is external to the curve shows the stable state $\alpha_i > 0$. The stability of the flow will generally be interpreted based on a critical Reynolds number, which indicates a more unstable flow when it is reduced. The eigenfunctions are then computed according to the boundary conditions (26) and (27). The stability of the flow is examined by plotting neutral points ($\alpha_i = 0$) in (R, F) plane, where $F = \omega/R$ is the scaled frequency of the disturbance.

Figures 9(a)–9(c) in this section present the effects of wall injection and suction on the neutral stability curves and data for a range of temperature dependencies. Note that the most amplified T-S disturbances appear near to the lower branch of the neutral curve in the boundary layer of the flat plate. Therefore, the structure of the T-S waves in the near-wall viscous layer are investigated. Figure 9(a) shows the neutral stability curves for $\varepsilon = -0.75$. Increasing f_w appears to stabilize the flow, as the critical Reynolds number is increased.

However, Fig. 9(c) shows the neutral stability curves for $\varepsilon = 0.75$, and different intensities of the suction ($f_w > 0$). In general, it can be noted that the scaled frequency of the disturbance reduces with increasing both f_w (suction) and ε . We note also that the critical Reynolds number increases with higher intensities of the suction, as seen in Table II. In this case, it is observed that increasing f_w causes a highly stabilising effect.

In contrast, in Fig. 9, we see that increasing the intensity of blowing leads to a marked leftward change of the curves, tending strongly toward lower Reynolds numbers. Thus, blowing appears to be highly destabilizing. Note that the region of instability is broadening greatly as the temperature-dependent viscosity becomes stronger or lower, although the curve of $\varepsilon = 0.75$ is more stable. We also note that the positive values of temperature cause greater leaps to lower Reynolds numbers, than negative temperature, which is evident in Fig. 9(a). From Table II, it is clear that the critical Reynolds number decreases sharply with higher intensities of injection for both increasing or decreasing ε .

Depending on our results of the mean flow profiles for Prandtl number effect in Sec. II, we note that the critical Reynolds number is increasing rapidly as Pr takes higher values. This means that the effect of increasing Prandtl number and flow suction shows a strongly stabilizing effect as seen in Fig. 10(b), whereas increasing flow injection exhibits a reverse effect as noted in Fig. 10(a). It is clear that significantly decreasing viscosity increases the Prandtl number value, leading to a more stabilizing effect, especially with increasing suction intensity.

IV. EIGENFUNCTION OF FLOW SUCTION AND INJECTION

We assess the eigenfunctions at $R_c + 200$, and find that the value of α used is that of the most amplified disturbance at this Reynolds number, which is found by marching through values of F within the neutral curve to find the maximum value of $-\alpha_i$.

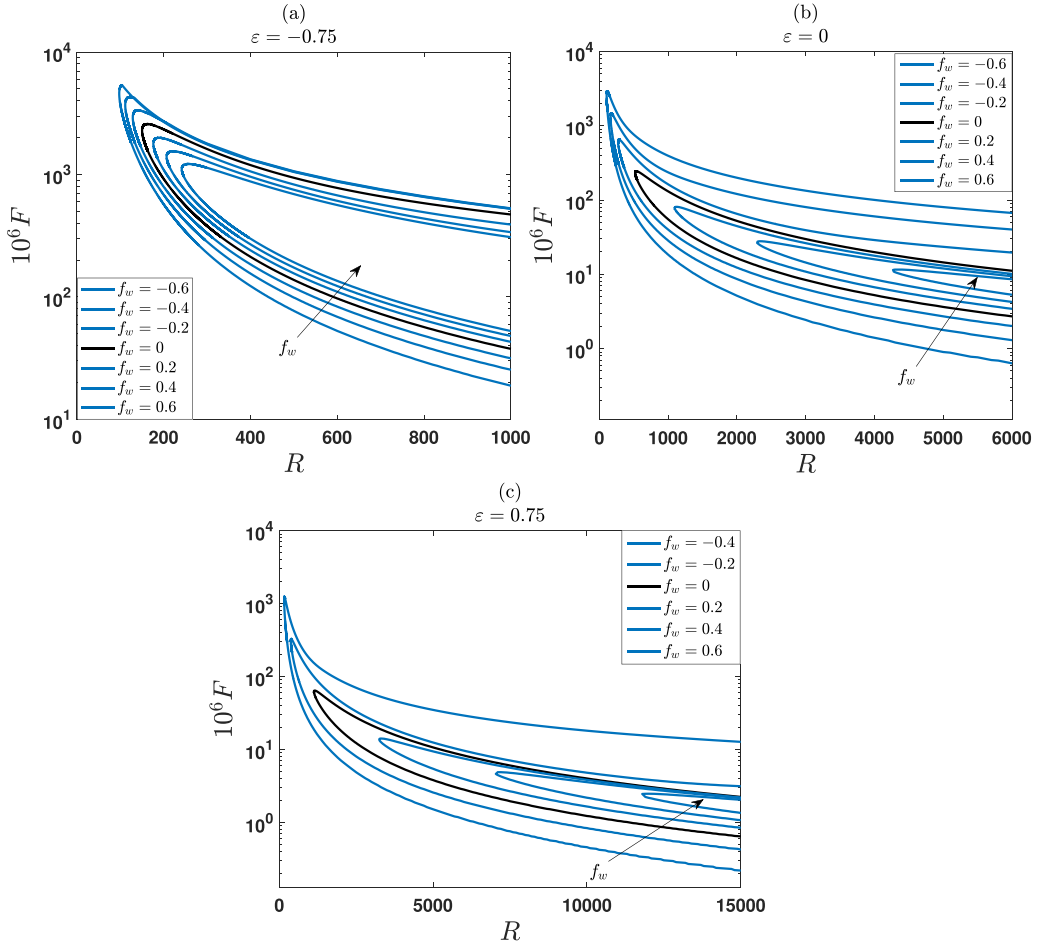


FIG. 9. Neutral curves, in cases of various suction and fixed $\varepsilon = -0.75, 0, 0.75$. (a) Neutral curves of suction at $\varepsilon = -0.75$. (b) Neutral curves of suction at $\varepsilon = 0$. (c) Neutral curves of suction at $\varepsilon = 0.75$.

Amplitudes of the perturbation stream function and streamwise, wall-normal, and temperature eigenfunctions for a range of ε values are combined with a fixed value of suction at ($f_w = 0.4$), and of injection at ($f_w = -0.4$), in Figs. 11 and 12, respectively. It can be seen that the profile maximum moves closer to the plate surface as ε and f_w are increased. This may be as a result of the narrowing of the corresponding mean flow profiles seen in Figs. 5–7. Wall and Wilson [30] observed a similar effect, and attributed it to the mean flow response of their temperature-dependent viscosity model.

Figure 11(a) exhibits the streamwise perturbation eigenfunctions for flow injection. It is noted that the typical shape of $|\tilde{u}(y)|$ moves away from the surface for $\varepsilon < 0$. The profile maximum is flattened at $\varepsilon = 0$ and $f_w = -0.4$. We can also see that $|\tilde{u}(y)|$ is sharply divided into two distinct maxima for $\varepsilon = -0.75$, and both maxima come together gradually to form one peak at $\varepsilon = 0$. Note that increasing ε and injection intensity acts to increase the maximum value of $|\tilde{u}(y)|$. In Fig. 11(b), the wall-normal disturbance eigenfunction with injection shows the same behavior seen with flow suction. However, here the profile moves away from the plate surface with increasing injection strength. The plots in Fig. 11(c) present a slight change of the maxima for $|\tilde{\Theta}(y)|$ with increasing ε which results in a movement closer to the surface.

Figure 12(a) shows the profile disturbance of $|\tilde{u}(y)|$, which is slightly divided into two distinct maxima for $\varepsilon = -0.75$. This division disappears gradually as ε and f_w are increased. However, the

TABLE II. Critical data for a range of the flow suction and injection intensity at fixed ε values.

f_w	R_c	$F \times 10^6$	$\alpha_{r,c}$
$\varepsilon = -0.75$			
-0.6	97.38	4613.88	0.8328
-0.4	111.23	3711.23	0.7649
-0.2	128.63	2929.33	0.7031
0	150.07	2298.26	0.6512
0.2	176	1789.77	0.605
0.4	206.53	1399.3	0.5658
0.6	241.4	1111.2	0.5360
$\varepsilon = 0$			
-0.6	104.70	2575.93	0.5508
-0.4	160.46	1340.52	0.4568
-0.2	271.35	607.70	0.3748
0	519	232.34	0.3044
0.2	1095.8	78.1	0.2474
0.4	2294	26.7	0.2056
0.6	4270	11.5	0.1862
$\varepsilon = 0.75$			
-0.6	80	3009.59	0.5255
-0.4	155.18	1125.14	0.4062
-0.2	373.07	308.79	0.3056
0	1125.30	62.12	0.2274
0.2	3250	13.88	0.1825
0.4	7040	4.64	0.1568
0.6	11800	2.47	0.1556

streamwise profile is maximum at $\varepsilon = 0.5$. In Fig. 12(b), we observe that the maximum value of $|\tilde{v}(y)|$ decrease with increasing ε . However, the turning point appears in the range $0.25 < \varepsilon < 0.75$. The magnitude of the temperature perturbation, $|\tilde{\Theta}(y)|$ shows a slight reduction toward the surface, as suction intensity and temperature dependence are increased, as is evident in Fig. 12(c). However, there are fluctuations in the maximum values beyond $\varepsilon = 0.25$.

V. ENERGY ANALYSIS

A. Formulation

The examination of the energetic input and output of disturbance to the mean flow depends on the eigenfunctions. Multiplying (19) and (20) by \hat{u} and \hat{v} , respectively, and then summing to form an equation representing the energy transfer processes of the system, leads to

$$\begin{aligned}
 & \hat{u} \frac{\partial \hat{u}}{\partial t} + \hat{v} \frac{\partial \hat{v}}{\partial t} + U \left(\hat{u} \frac{\partial \hat{u}}{\partial x} + \hat{v} \frac{\partial \hat{v}}{\partial x} \right) + U' \hat{u} \hat{v} \\
 & = - \left(\hat{u} \frac{\partial \hat{p}}{\partial x} + \hat{v} \frac{\partial \hat{p}}{\partial y} \right) + \frac{\bar{\mu}}{R} \left(\hat{u} \frac{\partial^2 \hat{u}}{\partial x^2} + \hat{u} \frac{\partial^2 \hat{v}}{\partial y^2} + \hat{v} \frac{\partial^2 \hat{u}}{\partial x^2} + \hat{v} \frac{\partial^2 \hat{v}}{\partial y^2} \right) \\
 & \quad + \frac{\bar{\mu}'}{R} \left(\hat{u} \frac{\partial \hat{v}}{\partial x} + \hat{u} \frac{\partial \hat{u}}{\partial y} + 2\hat{v} \frac{\partial \hat{v}}{\partial y} \right) + \frac{U'}{R} \left(\hat{u} \frac{\partial \hat{\mu}}{\partial y} + \hat{v} \frac{\partial \hat{\mu}}{\partial x} \right) + \frac{U'' \hat{u} \hat{\mu}}{R}.
 \end{aligned} \tag{28}$$

We define the following variables:

$$\hat{e} = \frac{1}{2} (\hat{u}^2 + \hat{v}^2), \quad \hat{q} = \frac{\partial \hat{v}}{\partial x} - \frac{\partial \hat{u}}{\partial y}, \quad \text{and} \quad \hat{s} = \frac{\partial \hat{v}}{\partial x} + \frac{\partial \hat{u}}{\partial y},$$

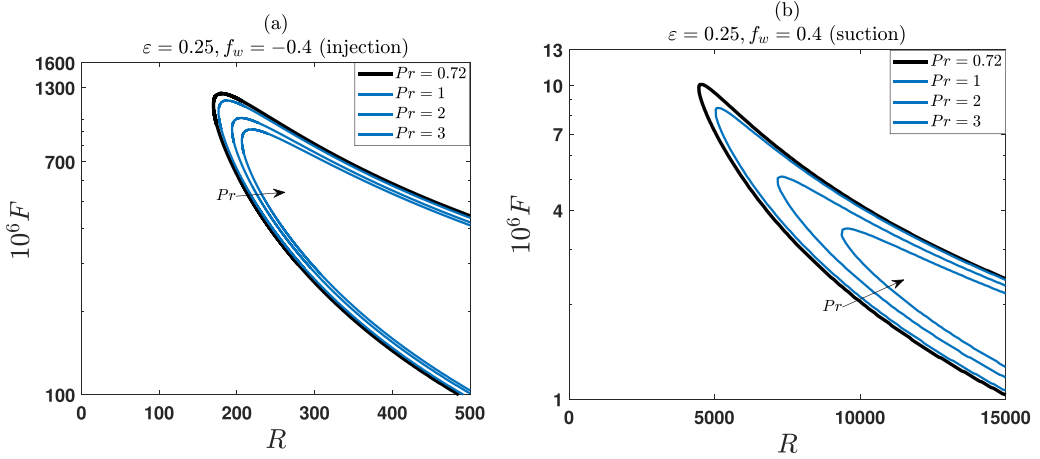


FIG. 10. Neural curves, in cases of a range of Prandtl number. (a) Neutral curves of Prandtl number at a fixed $f_w = -0.4$ (injection) and $\varepsilon = 0.25$. (b) Neutral curves of Prandtl number at fixed $f_w = 0.4$ (suction) and $\varepsilon = 0.25$.

where \hat{e} is the kinetic energy of the two disturbance quantities, \hat{q} is the disturbance vorticity and \hat{s} is defined purely for convenience. Following some manipulation of the term (28), the energy equation becomes

$$\begin{aligned} \left(\frac{\partial}{\partial t} + U \frac{\partial}{\partial x} \right) \hat{e} + U' \hat{u} \hat{v} = & - \frac{\partial(\hat{u} \hat{p})}{\partial x} - \frac{\partial(\hat{v} \hat{p})}{\partial y} + \frac{\bar{\mu}}{R} \left[\frac{\partial(\hat{v} \hat{q})}{\partial x} - \frac{\partial(\hat{u} \hat{q})}{\partial y} - \hat{q}^2 \right] \\ & + \frac{1}{R} \left\{ \bar{\mu}' \left[\frac{\partial(\hat{u} \hat{v})}{\partial x} + \frac{\partial(\hat{e} + \hat{v}^2)}{\partial y} \right] + U' \left[\frac{\partial(\hat{\mu} \hat{u})}{\partial y} + \frac{\partial(\hat{\mu} \hat{v})}{\partial x} - \hat{\mu} \hat{s} \right] + U'' \hat{\mu} \hat{u} \right\}. \end{aligned} \quad (29)$$

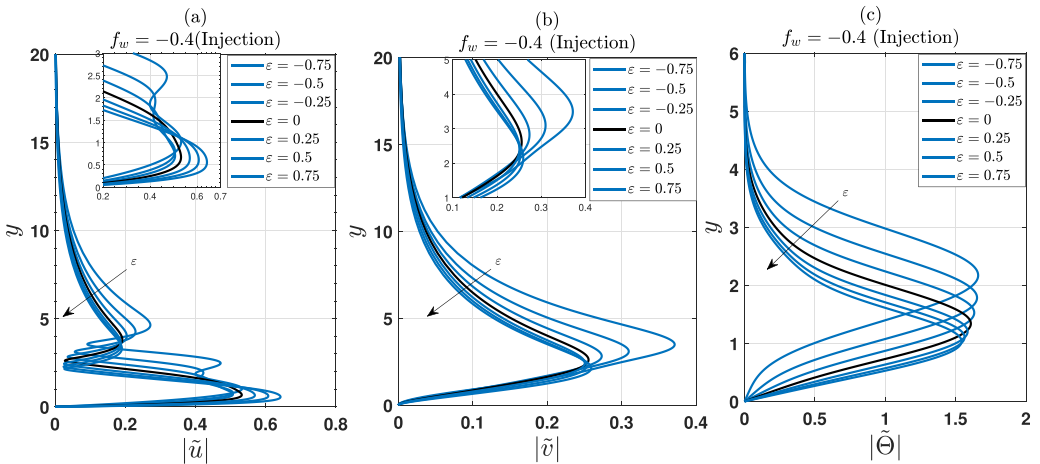


FIG. 11. Perturbation eigenfunctions for a range of temperature-dependent viscosity with fixed injection $f_w = -0.4$. (a) $|\tilde{u}|$ streamwise eigenfunctions. (b) $|\tilde{v}|$ plate normal eigenfunctions. (c) $|\tilde{\Theta}|$ temperature eigenfunctions.

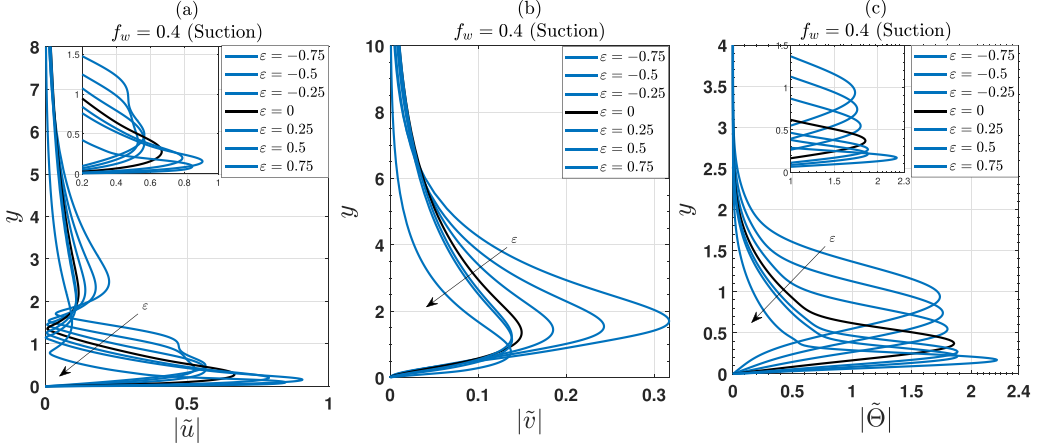


FIG. 12. Perturbation eigenfunctions for a range of temperature-dependent viscosity with fixed suction $f_w = 0.4$. (a) $|\tilde{u}|$ streamwise eigenfunctions. (b) $|\tilde{v}|$ plate normal eigenfunctions. (c) $|\tilde{\Theta}|$ temperature eigenfunctions.

Integration through the boundary layer results in the following integral energy equation:

$$\begin{aligned} \frac{dE}{dx} = & - \left\{ \int_0^\infty U' \langle \hat{u}\hat{v} \rangle dy \right\}^I + \frac{1}{R} \left\{ \frac{d}{dx} \int_0^\infty \bar{\mu} \langle \hat{v}\hat{q} \rangle dy - \int_0^\infty \bar{\mu} \langle \hat{q}^2 \rangle dy \right\}^{II} \\ & + \frac{1}{R} \left\{ \frac{d}{dx} \int_0^\infty \bar{\mu}' \langle \hat{u}\hat{v} \rangle + U' \langle \hat{\mu}\hat{v} \rangle dy + \int_0^\infty \bar{\mu}' \langle \hat{u}\hat{q} \rangle - \bar{\mu}'' (\langle \hat{e} + \hat{v}^2 \rangle) - U' \langle \hat{\mu}\hat{s} \rangle dy \right\}^{III}. \quad (30) \end{aligned}$$

The terms on the left-hand side of (30) represent the total mechanical energy E_t of the system, and here $E = \int_0^\infty U \langle \hat{e} \rangle + \langle \hat{u}\hat{p} \rangle dy$. The integral I represents energy production due to Reynolds stresses R_p , the integral II represents energy dissipation due to viscosity V_d , and terms in III represent additional terms arising from variable viscosity V_d . Hence the terms in III vanish when $\varepsilon = 0$.

B. Results of solutions

Note that for the integral energy solved via numerical integration we obtain the only non-negligible terms (on the left side) being I and the second term of II. However, all the terms in III are consistently negligible. The remaining terms are normalized with respect to $\int_0^\infty U \langle \tilde{e} \rangle + \langle \tilde{u}\tilde{p} \rangle dy$, as follows:

$$\underbrace{-2\alpha_i}_{E_t} \approx \underbrace{\int_0^\infty U' \langle \tilde{u}\tilde{v} \rangle dy}_{R_p} + \frac{1}{R} \underbrace{\int_0^\infty \bar{\mu} \langle \tilde{q}^2 \rangle dy}_{V_d}, \quad (31)$$

where $\tilde{e} = \frac{1}{2}(\tilde{u}^2 + \tilde{v}^2)$, $\tilde{q} = i\alpha\tilde{v} - \tilde{u}'$, and $\langle \tilde{x}\tilde{y} \rangle = \tilde{x}\tilde{y}^* + \tilde{x}^*\tilde{y}$, where a * refers to a complex conjugate.

The amplification of any turbulent eigenmode is noted when energy production outweighs energy dissipation.

Figure 13(a) represents the change in energy contributions generated by combined suction intensities with values of ε at $R_c(\varepsilon) + 200$. It can be seen that when $\varepsilon < 0$, the disturbances are significantly more amplified, while this amplification gradually decreases with increasing ε . However, when $\varepsilon > 0.25$, there are also significant fluctuations of amplification as f_w is increased.

Generally, the profiles of the energy loss from V_d are approaching zero as f_w and ε are increased. It can also be observed that all curves are not constant with a range of suction strengths. This means

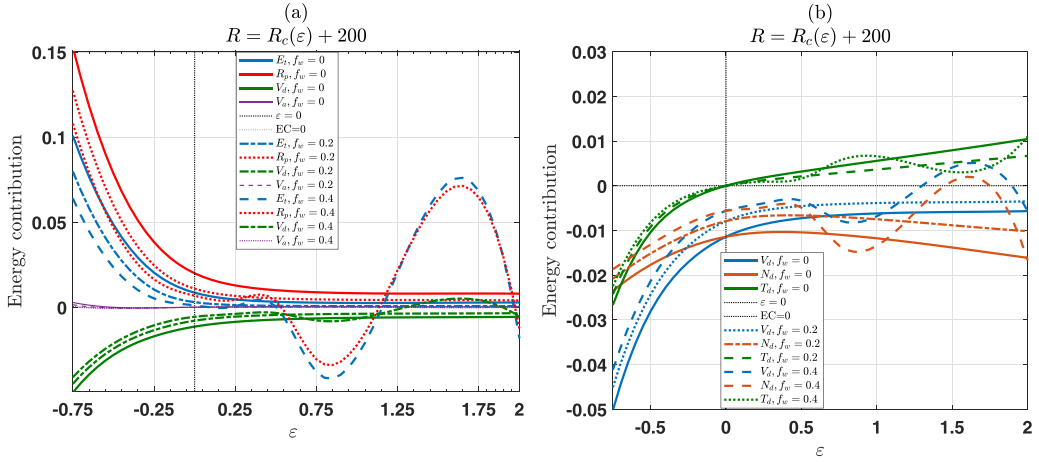


FIG. 13. (a) Component energy contributions and (b) total and component energy dissipation due to different suction values for a range of temperature dependencies. The vertical and horizontal black, dashed lines are provided as reference to $\varepsilon = 0$ and to zero energy contribution, respectively.

that the effects of wall suction combined with temperature-dependent viscosity are not consistent exactly with the effects of ε as is seen in Miller *et al.* [28].

In contrast, Fig. 14(a) shows an adverse change from that seen in Fig. 13(a), where all curves of the energy contribution and dissipation significantly move away from zero as the blowing intensity is increased.

We now separate V_d into a constant viscosity component and a temperature-dependent component, giving

$$\underbrace{\int_0^\infty \bar{\mu} \langle \hat{q}^2 \rangle dy}_{V_d} = \underbrace{\int_0^\infty \langle \hat{q}^2 \rangle dy}_{N_d} + \underbrace{\int_0^\infty (\bar{\mu} - 1) \langle \hat{q}^2 \rangle dy}_{T_d}. \quad (32)$$

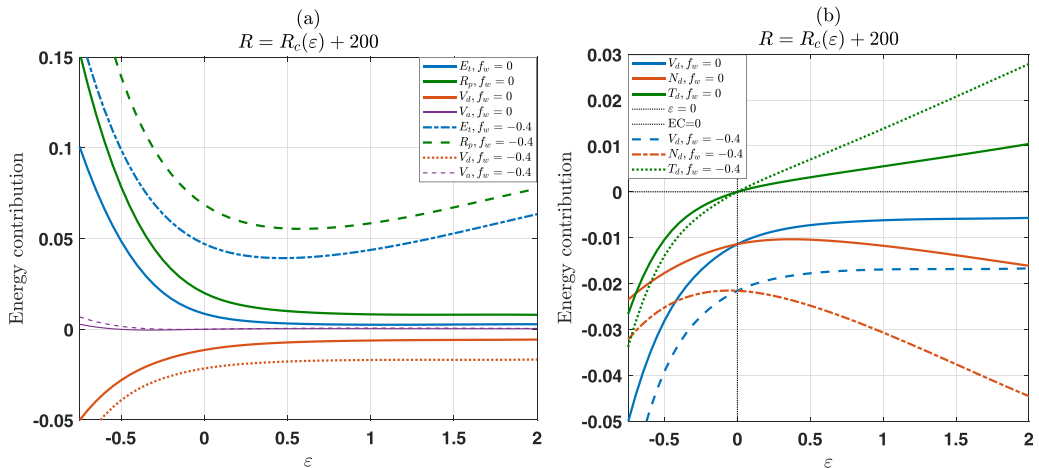


FIG. 14. (a) Component energy contributions and (b) total and component energy dissipation due to different blowing values for a range of temperature dependencies. The vertical and horizontal black, dashed lines are provided as reference to $\varepsilon = 0$ and to zero energy contribution, respectively.

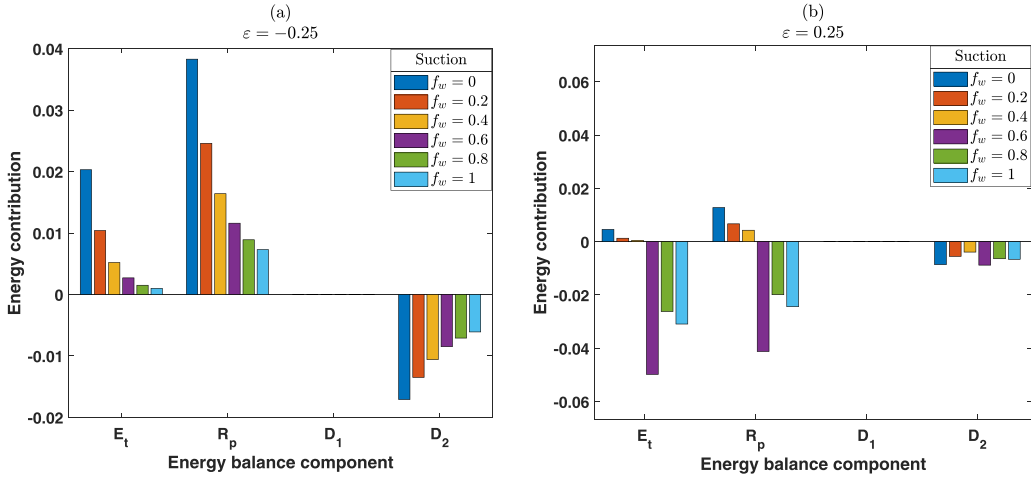


FIG. 15. Results of the energy balance integral showing the energy contribution of the individual components for a range of suction intensities with fixed ε . D_1 and D_2 are the first and second terms of V_d .

Here N_d indicates Newtonian dissipation, and T_d indicates temperature-dependent dissipation. This separation of V_d allows for further notes on how the variable's viscosity influences flow stability with suction.

Figure 13(b) shows the effects of flow suction as these two components interact over the range of temperature dependencies. The energy dissipation increases as suction intensities are increased. However, there are slight fluctuations of the energy contribution of V_d as $f_w > 0$.

Adversely, the energy contribution is unstable with increasing flow injection, as seen in Fig. 14(b). We see that both dissipation components are reduced for $f_w < 0$. The T_d curve is increased with injection capacity, i.e, dissipation for $\varepsilon < 0$ and production for $\varepsilon > 0$. The minimum

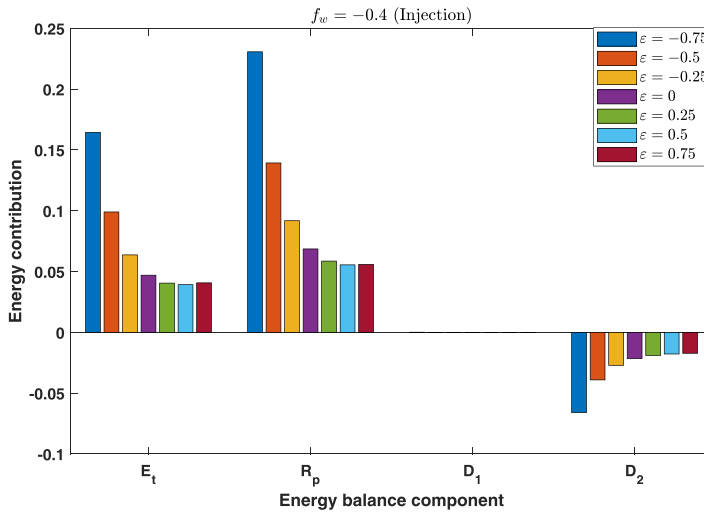


FIG. 16. Results of the energy balance integral showing the energy contribution of the individual components for a range of temperature dependencies with fixed injection f_w . D_1 and D_2 are the first and second terms of V_d .

dissipation exhibited by the N_d curve is also moved to a reduced value of temperature dependencies at a greater blowing intensity.

Figure 15(a) presents the energy balance calculation for $\varepsilon < 0$ and wall suction. This case shows the effects of suction for the energy production term R_p , the energy dissipation V_d , and the total mechanic energy E_t of the system, where it is noted that the total mechanic energy E_t is decreased as a result of reducing the energy production and the energy dissipation with increasing flow suction f_w and ε .

Figure 15(b) shows the energy balance calculation for a range of temperature-dependent viscosity $\varepsilon > 0$ and the suction. There is a stabilization effect on the T-S waves that mainly comes from the large reduction in the energy contribution term. Note that the significant invariance of the energy dissipation of the system V_d leads to a clear reduction in the total energy of the system as a result of increasing flow suction of this type. However, Fig. 16 displays a more destabilizing effect of flow injection as $f_w < 0$ and ε is decreased.

VI. SUMMARY OF THE CURRENT RESULTS

This paper has been designed to analyze the effects of wall suction and injection on the stability of the Blasius boundary-layer flow over a heated and permeable plate with a temperature-dependent viscosity flow.

In Sec. II, we summarized and discussed the results of the effects of flow suction on boundary-layer flow over a heated plate as follows: Our theoretical analysis depended on the no-penetration condition modification for formulating the steady boundary-layer flow over a permeable, heated, plate. Formulations of and solutions to the mean flow equations are formatted for various temperature dependencies. The results exhibit a reduction in the boundary-layer flows of the mean flow profile toward the plate surface, in particular with decreasing viscosity and increasing suction intensity. Therefore, the effects of the suction show a more steady state of boundary-layer flows with decreasing viscosity via setting $\varepsilon > 0$. We see also that increasing Prandtl number with flow suction results in a greater reduction the temperature profile when $\varepsilon > 0$.

Our analysis of linear stability based on the steady mean flow reveals that flow suction has a strong, stabilizing effect, which is shown in lower viscosity as presented in Sec. III. Overall, our findings are consistent with those presented by Laouar *et al.* [19] and Miller *et al.* [28] for the smooth heated plate, respectively.

In Sec. V, our study revealed that wall suction acts to reduce energy production of the T-S instabilities. In contrast, there is a sharply destabilizing effect with increasing flow injection and viscosity.

We briefly consider our results in the context of CVD reactor flows. Note that the temperature dependence of a gas viscosity is given by setting $\varepsilon < 0$ and that the upper limit of operation of a CVD reactor returns flows with $R \sim 200$. Based on the viscosities at 300 K and 1300 K under atmospheric pressure for context [31], a dry-air value is represented by $\varepsilon \approx -0.62$ according to the inverse linear model.

From Table II, we see that the lower limit of $\varepsilon = -0.75$, $R_c \approx 97, 111, 128$, in a range of injection intensity. This means that the flow of a gas mixture used in a CVD reactor with its susceptor designed by wall injection has a viscosity-temperature relationship within the parameter range where the critical Reynolds number characteristic of linear instability appears for $R < 200$. It is clear in this case that wall injection is destabilizing to the flow.

The results presented in this paper have shown that introducing wall suction is stabilizing to the flow, though Fig. 9(a) shows that this stabilizing effect is significantly diminished for $\varepsilon = -0.75$ and $f_w < 0.4$. We re-examine Fig. 9(a) and find that for $\varepsilon = -0.62$, $R_c(f_w = 0) \approx 150$ and $R_c(f_w = 0.4) \approx 206$. Therefore, the analysis presented here shows that a gas mixture used in a CVD reactor with its susceptor designed using a small suction intensity could have a viscosity-temperature relationship within the parameter range where linear instability appears for $R < 200$. Furthermore, results indicate that this slight suction effect may be stabilizing.

The current formulation could be developed by other techniques to model flows within a CVD reactor. Jensen *et al.* [27] indicates there is a need for temperature-dependent density to reflect gas expansion in the context of a CVD reactor. However, by approximating constant Pr and C_p (both show little variation with temperature) noted by Kays and Crawford [32], other properties of temperature-dependent gas, e.g., ρ , can be interpreted as “compensating” for each other. In this case, the same steady-mean flow equations derived in this study for the heated, permeable plate can be obtained and an incompressible approximation may be considered. The Blasius approximation in this study is quite similar to a Poiseuille one for metal-organic chemical vapor deposition reactors [33,34].

Nevertheless, an extension of the work presented in this study to form a comparison that fully incorporates the temperature dependence of each physical property of the fluid is required to confirm which of these approximations have suitable grounds for justification. In this light, similarly to Ref. [34], we plan to extend our analysis to consider the effects of temperature dependence on density, and we hope to report on this in the future.

Miller *et al.* [28] indicates the reaction mechanisms in CVD reactors are multistaged and complex, and the most rigorous analysis needs multiple-interacting-species continuity equations for each stage. However, a CVD reactor in its processes depends on reactants that are typically very dilute compared to carrier gases. For this reason, the single diffusion equation can be used to track all chemical species by making a no gas-phase reactions approximation [25]. Consistent with this approximation, the different diffusive responses of the particle mixture to the temperature gradient can be investigated by utilizing the Soret effect [35].

ACKNOWLEDGMENTS

M.A.-M. wishes to gratefully acknowledge support from the Saudi Arabian Cultural Bureau in the UK and a scholarship sponsored by University of Taif in Saudi Arabia. Z.H. wishes to acknowledge support from the EPSRC under Grant No. EP/R028699/1. The authors wish to thank the referees for their useful comments and suggestions to improve on an earlier draft of this paper.

-
- [1] F. Thierry and C. Grégoire, Cannel flow induced by wall injection of fluid and particles, *Phys. Fluids* **15**, 348 (2003).
 - [2] M. E. Goldstein and L. S. Hultgren, Boundary layer receptivity to longwave free-stream disturbances, *Annu. Rev. Fluid Mech.* **21**, 137 (1989).
 - [3] H. W. Liepmann and G. L. Brown, Active control of laminar-turbulent transition, *J. Fluid Mech.* **118**, 201 (1982).
 - [4] M. Miklavčič and C. Wang, The flow due to a rough rotating disk, *Z. Angew. Mat. Phys.* **55**, 235 (2004).
 - [5] T. Wiegand, H. Bestek, and S. Wagner, Transition process of a wave train in a laminar boundary layer, in *New Results in Numerical and Experimental Fluid Mechanics* (Springer, Berlin, 1997), Vol. 60, p. 397.
 - [6] P. Ricco and F. Dilib, The influence of wall suction and blowing on boundary-layer laminar streaks generated by free-stream vortical disturbances, *Phys. Fluids* **22**, 1 (2010).
 - [7] Z. Mehrez, M. Bouterra, A. E. Cafsi, A. Belghith, and P. L. Quere, Enhancement of heat transfer in turbulent separated and reattached flow by a periodic perturbation, *Int. J. Heat Technol.* **27**, 23 (2009).
 - [8] N. Ahmed and H. Kalita, Mhd oscillatory free convective flow past a vertical plate in slip-flow regime with variable suction and periodic plate temperature, *Int. J. Heat Technol.* **30**, 97 (2012).
 - [9] K. Kim and H. J. Sung, Effects of periodic blowing from spanwise slot on a turbulent boundary layer, *AIAA J.* **41**, 1916 (2003).
 - [10] J. Park and H. Choi, Effects of uniform blowing or suction from a spanwise slot on a turbulent boundary layer flow, *Phys. Fluids* **11**, 3095 (1999).
 - [11] K. Kim, M. K. Chung, and H. J. Sung, Assessment of local blowing and suction in a turbulent boundary layer, *AIAA J.* **40**, 175 (2002).

- [12] A. Pantokratoras, Laminar free-convection over a vertical isothermal plate with uniform blowing or suction in water with variable physical properties, *Int. J. Heat Mass Transf.* **45**, 963 (2002).
- [13] J. L. Bansal, Heat and mass transfer in a laminar boundary layer on a flat plate with variable suction or injection velocity and constant wall temperature, *Int. J. Heat Mass Transf.* **12**, 173 (1969).
- [14] M. E. Ali, The effect of suction or injection on the laminar boundary layer development over a stretched surface, *J. King Saud Univ. Eng. Sci.* **8**, 43 (1996).
- [15] M. M. T. Hossaina, B. Mandalb, and M. A. Hoossaina, Similarity solution of unsteady combined free and force convective laminar boundary layer flow about a vertical porous surface with suction and blowing, *Proc. Eng.* **56**, 134 (2013).
- [16] N. A. A. Bakara, N. Bachokb, N. M. Arifinb, and I. Popc, Stability analysis on the flow and heat transfer of nanofluid past a stretching/shrinking cylinder with suction effect, *Results Phys.* **9**, 1335 (2018).
- [17] A. Laouara and E. H. Mezaacheb, Numerical study of the effect of parietal suction and injection on momentum and heat transfer of laminar and turbulent external flow, *Energy Proc.* **36**, 1101 (2013).
- [18] M. H. Shojaefard, A. R. Noorpoor, A. Avanesians, and M. Ghaffarpour, Numerical investigation of flow control by suction and injection on a subsonic airfoil, *Am. J. Appl. Sci.* **2**, 1474 (2005).
- [19] A. Laouer, E. H. Mezaache, and S. Laouar, Study of the effect of parietal suction and blowing on the stability of laminar external flow, *Int. J. Heat Technol.* **34**, 302 (2016).
- [20] H. Blasius, Grenzschichten in flüssigkeiten mit kleiner reibung, *Z. Angew. Math. Phys.* **56**, 1 (1908).
- [21] W. Tollmien, Über die entstehung der turbulenz, *Nachr. Ges. Wiss. Göttingen Math.-Phys. Kl II*, **21** (1929).
- [22] H. Schlichting, Laminare strahlausbreitung, *Zeitschr. Angew. Math. Mech.* **13**, 260 (1933).
- [23] H. K. Schubauer and G. B. Skramstrad, Laminar boundary-layer oscillations and stability of laminar flow, *Aeronaut. J.* **14**, 69 (1947).
- [24] J. R. Lloyd and E. M. Sparrow, On the instability of natural convection flow on inclined plates, *J. Fluid Mech.* **42**, 465 (1970).
- [25] W. L. Holstein, Design and modeling of chemical vapor deposition reactors, *Prog. Cryst. Growth Charact. Mater.* **24**, 111 (1992).
- [26] C. R. Kleijn, On the modelling of transport phenomena in chemical vapour deposition and its use in reactor design and process optimization, *Thin Solid Films* **206**, 47 (1991).
- [27] K. F. Jensen, E. O. Einset, and D. I. Fotiadis, Flow phenomena in chemical vapor deposition of thin films, *Annu. Rev. Fluid Mech.* **2**, 197 (1991).
- [28] R. Miller, S. J. Garrett, P. T. Griffiths, and Z. Hussain, Stability of the blasius boundary layer over a heated plate in a temperature-dependent viscosity flow, *Phys. Rev. Fluids* **3**, 113902 (2018).
- [29] H. Schlichting, *Boundary-layer Theory*, 7th ed. (McGraw–Hill, New York, 1979).
- [30] D. P. Wall and S. K. Wilson, The linear stability of flat-plate boundary-layer flow of fluid with temperature-dependent viscosity, *Phys. Fluids* **9**, 2885 (1997).
- [31] Engineering Toolbox, Dry air properties <https://www.engineeringtoolbox.com/dry-air-properties-d-973.html>
- [32] M. E. Kays and W. M. Crawford, *Convective Heat and Mass Transfer*, 3rd ed. (McGraw–Hill, New York, 1993).
- [33] J. V. D. Ven, G. M. J. Rutten, M. J. Raaijmakers, and L. J. Giling, Gas phase depletion and flow dynamics in horizontal mocvd reactors, *J. Cryst. Growth* **76**, 352 (1986).
- [34] P.-Y. Lagrée, Thermal mixed convection induced locally by a step change in surface temperature in a poiseuille flow in the framework of Triple Deck theory, *Int. J. Heat Mass Transf.* **31**, 2509 (1999).
- [35] J. K. Platten, The soret effect: A review of recent experimental results, *J. Appl. Mech.* **73**, 5 (2006).